Precipitation efficiencies in a climatology of Southern Ocean extratropical cyclones

Article

Published Version

Creative Commons: Attribution 4.0 (CC-BY)

Open Access

Dacre, H. F. ORCID: https://orcid.org/0000-0003-4328-9126, Martinez-Alvarado, O. ORCID: https://orcid.org/0000-0002-5285-0379 and Hodges, K. I. ORCID: https://orcid.org/0000-0003-0894-229X (2023) Precipitation efficiencies in a climatology of Southern Ocean extratropical cyclones. Journal of Geophysical Research: Atmospheres, 128 (24). e2023JD039239. ISSN 2169-8996 doi: 10.1029/2023JD039239 Available at https://centaur.reading.ac.uk/114224/

It is advisable to refer to the publisher's version if you intend to cite from the work. See Guidance on citing.

To link to this article DOI: http://dx.doi.org/10.1029/2023JD039239

www.reading.ac.uk/centaur

CentAUR

Central Archive at the University of Reading

Reading's research outputs online

JGR Atmospheres

Precipitation Efficiencies in a Climatology of Southern Ocean Extratropical Cyclones

H. F. Dacre[1] [iD], O. Martinez-Alvarado[2] [iD], and K. I. Hodges[1,2]

[1]Department of Meteorology, University of Reading, Reading, UK, [2]National Centre for Atmospheric Science, University of Reading, Reading, UK

Abstract Precipitation efficiency refers to the amount of water that is lost from the atmosphere through precipitation compared to the available water vapor in the atmosphere. This metric plays a critical role in understanding precipitation patterns. However, calculating precipitation efficiency for extratropical cyclones can be challenging because cyclones are dynamic and move through the atmosphere as they evolve. To overcome this challenge, our study uses ERA5 reanalysis data to estimate precipitation efficiencies for 400 Southern Ocean cyclones, with a frame of reference that moves with the individual cyclones. Our findings indicate that at maximum intensity, average precipitation efficiencies reach a maximum of 60%/6 hr near the warm front where ascent rates are the largest. Typically, within 24–36 hr after cyclogenesis, all of the initial water vapor available within 500 km of a cyclone center is lost due to precipitation. However, a cyclone's precipitating phase is prolonged due to local evaporation and moisture flux convergence (MFC), which replenish the moisture lost via precipitation. Close to the cyclone center, MFC provides additional moisture from the environment into which cyclones are traveling. On average, this extends a cyclone's precipitation phase to over 60 hr after cyclogenesis. Thus, while moisture from the genesis location is quickly removed from the cyclone via precipitation, cyclones are replenished by moisture along their track, which doubles the timescale for a cyclone's precipitating phase.

Plain Language Summary Precipitation efficiency is a measure of how much water in the atmosphere falls as rain compared to how much is available to fall. In this study, we estimate how efficient precipitation is for 400 cyclones in the Southern Ocean. We find that when the cyclones are strongest, about 60% of the available water vapor turns into rain every 6 hr near the warm front of the cyclone where air is rising rapidly. Normally, within a day or two of a cyclone forming, all of the available water vapor in the cyclone gets turned into rain. However, the rain can persist for longer because cyclones pick up more moisture as they move, which gets turned into more rain. This can make the rain from a cyclone last on average for 60 hr, even after the initial moisture is all gone.

1. Introduction

The precipitation associated with extratropical cyclones can lead to extensive flooding causing damage to life, infrastructure, crops, and property. In the subtropics cyclone intensity is a good predictor of cyclone precipitation accumulation since moisture is readily available for conversion into precipitation (Pfahl & Sprenger, 2016). However, in the extratropics, the availability of moisture is limited and so becomes an important factor in cyclone precipitation totals. Since cyclones usually travel polewards during their lifecycle, the availability of moisture typically reduces. Thus, an interesting feature of extratropical cyclones is that their precipitation maximum generally occurs prior to their maximum dynamical strength either due to reduced moisture availability or due to the diabatic heating that occurs within the maximum precipitation phase further enhancing the dynamical intensity of cyclones (Bengtsson et al., 2009; Booth et al., 2018). The mean flow in the extratropics is approximately zonal with most meridional transport of moisture occurring in the vicinity of extratropical cyclones. This meridional transport of moisture occurs in filaments of high water vapor flux within the warm sector of extratropical cyclones, known as atmospheric rivers (Newell et al., 1992). Sinclair and Dacre (2019) showed that at 50°S, a cyclone's genesis latitude is the most important factor in determining the amount of moisture a cyclone transports to this latitude, but at 65°S, genesis latitude is no longer a significant factor. In this study we will explore the reason for this and test the hypothesis that as cyclones travel poleward the original moist air at cyclogenesis is replaced by moisture evaporated from higher latitudes. In particular, we aim to answer the following questions. How long would it take to deplete all of a cyclone's initial moisture via precipitation? If local evaporation or

moisture flux convergence (MFC) into the cyclone occurs, then replenishment of the cyclone's moisture content takes place. By how much does this moisture replenishment extend the precipitating phase of a cyclone? Finally, from where does the moisture leading the replenishment originate?

Several studies have performed moisture tagging using model data to quantify the contribution of subtropical moisture to the Total Column Water Vapor (TCWV) or precipitation when atmospheric rivers reach land. The ratio of subtropical moisture to the TCWV or precipitation at landfall is on average 25% (Hu & Dominguez, 2019), but for individual cyclones ranges from 10% for moisture transported more than 30°N latitude from their genesis latitude before making landfall (Sodemann & Stohl, 2013) to over 50% for moisture transported less than 15°N latitude from their genesis latitude before making landfall (Eiras-Barca et al., 2017; Rea et al., 2023). Thus, the contribution of sub-tropical moisture is highly variable from case-to-case but typically decreases the further the cyclones travel from the subtropics. These studies assume that evaporation or convergence of local moisture along the cyclone path is responsible for the remaining moisture or precipitation.

The relative contribution from evaporation or convergence and how they vary as the cyclones evolve can be quantified using the moisture budget. The ratio of different terms in the moisture budget allows replenishment or drying efficiencies to be determined. Precipitation efficiency (PE) refers to the ratio of the water that is lost from the atmosphere through precipitation to the available moisture in the atmosphere. It can be calculated on a global domain, using monthly or annual averaged values (Tuller, 1971) or for an individual moving mesoscale or synoptic-scale feature such as a thunderstorm, tropical or extratropical cyclone using instantaneous or accumulated values. There are many ways of estimating the PE depending on the method used to determine the available moisture. These include estimates of total column water vapor (Lutz, 1977; Stewart, 1996), condensation rate (Ferrier et al., 1996; Hobbs et al., 1980), moisture inflow (MFC) (Browning & Harrold, 1970), total column water vapor plus MFC (Guo et al., 2015), and evaporation plus MFC (Li et al., 2002). The range of methods and variation in accumulation periods makes comparison between studies difficult. For example, Hobbs et al. (1980) calculate precipitation efficiencies, using instantaneous precipitation and condensation rates. They find precipitation efficiencies of 40%–50% for a warm sector rainband and precipitation efficiencies of up to 80% in their cold-frontal rainband. Guo et al. (2015) calculate precipitation efficiencies as the ratio of accumulated precipitation over a 10 hr period to the accumulated evaporation and MFC over the same period. They estimated that the PE was 67% in the warm sector of the cyclone they studied. While the exact numerical values in these studies cannot be compared, studies generally agree that precipitation efficiencies are relatively high in the vicinity of individual extratropical cyclones studied. In this study, we will extend this analysis to estimate precipitation efficiencies for a whole climatology of cyclones.

High precipitation efficiencies indicate that moisture is rapidly lost from cyclones resulting in a short precipitation phase. However, observations show that cyclones typically precipitate for longer than one day. Therefore, moisture must be supplied to the cyclone to extend the precipitation phase. Previous studies investigating moisture convergence near cyclones have identified the feeder airstream (FA) as an important low-level airflow for transporting moisture into and out of the center of cyclones and thus leading to the replenishment or depletion of moisture. It has been found that moisture at the head of an atmospheric river accelerates towards the cyclone center in the anticyclonically turning branch of the FA, feeding moisture to the base of the warm conveyor belt (WCB) where it then rises to form precipitation (Bui & Spengler, 2021; H. F. Dacre et al., 2019; Demirdjian et al., 2022; Papritz et al., 2021). Conversely, moisture in the remainder of the atmospheric river travels slower than the cyclone propagation speed resulting in the export of moisture from the cyclone by the cyclonically turning branch of the FA (Cuckow et al., 2022; H. F. Dacre et al., 2015; Xu et al., 2022). In this study, we will determine the extent to which low-level cyclone airflows redistribute moisture around cyclones, leading to the increase or decrease of general precipitation efficiencies.

2. Method

2.1. ERA5 Data

In this study, we use the European Center for Medium-Range Weather Forecasts (ECMWF) fifth generation reanalysis data set (ERA5). It provides a comprehensive view of the state of the Earth's atmosphere, land surface, and oceans, by assimilating observational data from a variety of sources, including satellite data, weather balloons, and weather stations (Hersbach et al., 2020). The ERA5 surface parameters used in this study are precipitation and
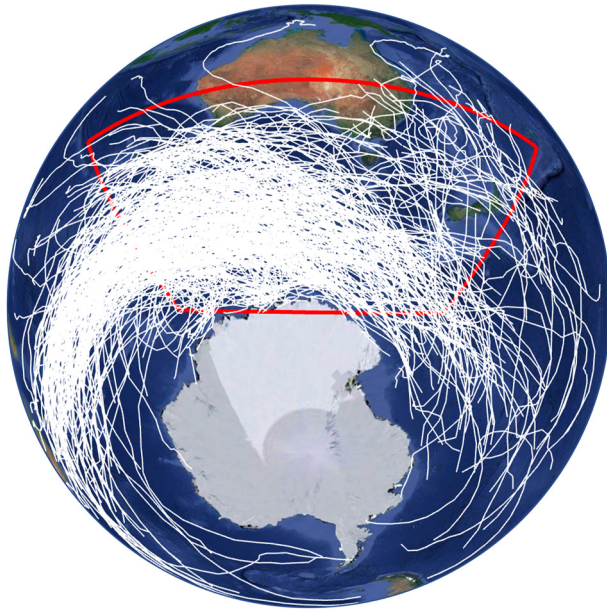
Figure 1. Tracks of 400 most intense extratropical cyclones in the ERA5 data set between March and September 1979–2021 with maximum intensity in the Southern Ocean surrounding Australia (90°–180°E, 20°–60°S, red box).

evaporation. They are extracted on a latitude-longitude grid with a resolution of 0.25° Precipitation is the combined liquid and frozen water that descends onto the Earth's surface, comprising both large-scale precipitation and convective precipitation. Large-scale precipitation is produced by the cloud scheme within the ECMWF Integrated Forecasting System (IFS), which models the formation and dissipation of clouds and large-scale precipitation as a result of alterations in temperature, pressure, and moisture at scales larger than the grid box. Convective precipitation is generated by the convection scheme in the IFS, which represents convection at scales smaller than the grid box. Evaporation is the cumulative amount of water that has vaporized from the Earth's surface. Lavers et al. (2022) evaluated ERA5 precipitation against 5,637 stations observations over 2001–2020. They conclude that globally there is a small wet bias in ERA5 precipitation, but that errors are smallest in winter extratropical areas. Since our study focuses on winter extratropical cyclones, we use ERA5 precipitation as a proxy for observed precipitation. Specific humidity, meridional and zonal components of the wind are extracted on isobaric surfaces on a longitude-latitude grid with a resolution of 0.25°. To determine moisture flux on isobaric surfaces, a 6-hourly temporal resolution was utilized.

2.2. Cyclone Identification

Based on the study by H. Dacre et al. (2012), we have tracked the location of the 400 most intense cyclones over a period of 42 years (1979–2021) using the tracking algorithm developed by Hodges (1995). The tracking process was carried out during the extended austral winter (May-September), and hourly 850 hPa relative vorticity. Since relative vorticity is a noisy field, before performing the tracking the vorticity field is spectrally truncated to T63. T63 corresponds to a resolution on a Gaussian grid of approximately 1.88° at the equator. The tracked vorticity features were filtered to exclude short-lived (<48 hr lifetime) or stationary features (traveling <1,000 km in their lifetime) unrelated to extratropical cyclones. Cyclogenesis is defined as the first identified point in each cyclone track. The intensity of the cyclones was measured using the maximum T63 vorticity. The 400 most intense cyclone tracks that attain their maximum intensity in the oceans surrounding Australia (90°–180°E, 20°–60°S) are illustrated in Figure 1. Our focus on this region is because extratropical cyclones in this area typically occur over the ocean, and thus they are closer to idealized aquaplanet conditions, and because there is a lack of cyclone studies conducted in the Southern Hemisphere.

2.3. Cyclone Compositing

To extract the fields used in this study, ERA5 data was obtained at 6-hourly intervals for each of the cyclone's locations within a 20° radius of the cyclone center. Following Catto et al. (2010), cyclone-relative composites were generated by averaging over all cyclones, after the fields were rotated to align with the direction of travel of each cyclone. The direction of travel was estimated using the position 6 hr earlier and 6 hr later. This rotation is crucial because cyclones have varying propagation directions. It improves the alignment of mesoscale features such as warm and cold fronts, which can be smoothed out completely during compositing if rotation is not performed. Only the 400 most intense cyclones were included in the composite, as this method assumes that all cyclones intensify and decay at similar rates. Limiting the number of cyclones produced a more homogeneous group with regard to their evolution but may bias the mean fields to be representative of the most intense cyclones.

2.4. Water Vapor Budget

To investigate the role of precipitation, evaporation, and MFC in regulating the moisture content of extratropical cyclones, we computed the individual contributions of these terms to the water vapor budget for each gridbox column within the cyclone system. The water vapor budget in a column of air was determined by the following equation:

$$P + E + MFC = \frac{1}{g} \int_{p_1}^{p_2} \frac{\partial q}{\partial t} dp, \tag{1}$$

$$MFC = -\frac{1}{g}\int_{p_1}^{p_2} \nabla \cdot \left(q\vec{u}\right)dp. \tag{2}$$

P is the surface precipitation flux in units of kg m^{-2}s^{-1} and is defined to be negative in this study, E is the surface evaporation flux in units of kg m^{-2}s^{-1} (positive values indicate evaporation and negative values indicate condensation in this study), g is the acceleration due to gravity in units of m s^{-2}, q is the specific humidity in units of kg kg^{-1}, t is time in units of seconds, and $\vec{u}$ is the horizontal wind vector in units of m s^{-1}. The vertically integrated terms are integrated from $p_1 = 1{,}000$ hPa to $p_2 = 200$ hPa. The third term on the left-hand side of Equation 1 represents the vertically integrated MFC and is given in Equation 2. The term on the right-hand side of Equation 1 represents the vertically integrated rate of change of water vapor in the column, positive values indicate moistening and negative values indicate drying columns of air.

2.5. Moisture Efficiencies and Depletion Timescales

In Section 4 we calculate the moisture efficiencies over a 6-hr period at each gridpoint in the domain surrounding the cyclone center. The PE, evaporation efficiency (EE) and MFC efficiency (MFCE) at time t are the first 3 terms in Equation 1 accumulated over a 6-hr period, divided by the TCWV at the start of the 6-hr period ($t - 6$).

$$PE = \frac{P_t}{TCWV_{t-6}},$$
$$EE = \frac{E_t}{TCWV_{t-6}}, \tag{3}$$
$$MFCE = \frac{MFC_t}{TCWV_{t-6}}.$$

The PE is negative and represents the percentage of TCWV removed by precipitation over 6 hr. The EE is positive, and represents the percentage of TCWV replenished by evaporation over 6 hr. The MFC efficiency can be positive or negative and represents the percentage of TCWV either replenished or removed over 6 hr respectively, depending on whether MFC or moisture flux divergence occurs at each location. The sum of the efficiencies is used to determine whether the columns are moistening or drying over the 6-hr period.

In Section 6 we calculate the timescale over which the moisture in a cyclone would completely 'dry out' due to the accumulated precipitation integrated over a circle with radius r from the cyclone center. We refer to this as the precipitation depletion timescale, PDT. When calculating the PDT we assume that any cloud microphysical processes in the precipitation process, due to the addition or removal of moisture by evaporation and MFC, do not result in significant systematic changes to the climatological PDT. The PDT is calculated relative to the TCWV in the cyclone system at the cyclogenesis time, t_0, such that;

$$\frac{\sum_{t=t_0}^{PDT}\int_0^r \int_0^{360} P_t\, dr\, d\theta}{\int_0^r \int_0^{360} TCWV_{t_0}\, dr d\theta} = -1 \tag{4}$$

The moisture lost from the cyclone system via precipitation may be replenished due to evaporation as the cyclone evolves. Moisture may also be replenished or depleted from the cyclone if the MFC is positive or negative respectively. Thus the general depletion timescale, GDT, is given by;

$$\frac{\sum_{t=t_0}^{GDT}\int_0^r \int_0^{360} (P_t + E_t + MFC_t)\, dr\, d\theta}{\int_0^r \int_0^{360} TCWV_{t_0}\, dr\, d\theta} = -1 \tag{5}$$

3. Composite Cyclone Structure

In this section, we depict the composite fields of cyclones during various stages of their evolution. In general, the cyclone lifetime is split into a developing and decaying phase (although some cyclones can undergo multiple deepening phases). The distribution of cyclone lifetimes for the 400 cyclones in the climatology is non-Gaussian with a few cyclones having very long lifetimes, so we calculate the mode of the distribution to represent the
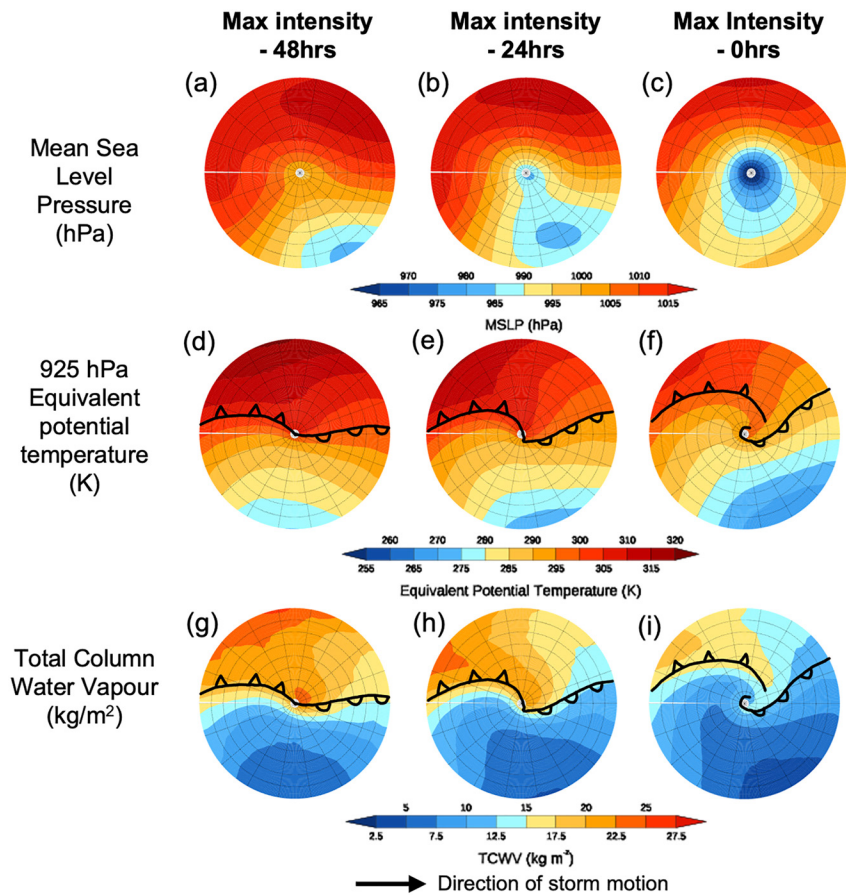
Figure 2. Evolution of cyclone centered composite fields overlaid with fronts (black). (a–c) Mean sea level pressure (hPa), (d–f) 925 hPa Equivalent potential temperature (K), (g–i) Total column water vapor (kg m^{-2}). Fields are shown at maximum intensity (right column), 24 hr before maximum intensity (middle column) and 48 hr before maximum intensity (left column). Images available from the Southern Hemisphere Storms Atlas, www.met.reading.ac.uk/~storms.

average cyclone characteristics. The average cyclone lifetime is 102 hr and the average time for a cyclone to reach maximum intensity after cyclogenesis is 42 hr. Since we are interested in studying the cyclone's precipitating phase, we also calculate the time of maximum precipitation, which occurs on average 24 hr prior to maximum intensity. To illustrate this stage of the cyclone evolution we analyze fields 48 and 24 hr prior to maximum intensity, and at maximum intensity.

Figures 2a–2c illustrate the composite mean sea level pressure (mslp) evolution during the developing stage of cyclone evolution. At 48 hr before the cyclones attain maximum intensity a trough extends toward the center of the cyclone. There is a minimum mslp of 998 hPa at the center of the composite cyclone but the lowest pressure within the 2,000 km radius domain is located to the south-east of the cyclone center. This is a possible parent cyclone (H. F. Dacre & Pinto, 2020; Hoskins & Hodges, 2005) with a frontal wave cyclone developing along the parent cyclone's trailing cold front. At 24 hr before maximum intensity, the composite cyclone has formed a closed mslp contour. There is still a low-pressure region to the south-east of the cyclone center, but it is closer to the cyclone of interest. Finally, at maximum intensity, the mslp at the cyclone's center has decreased by a further 15 hPa, to 970 hPa. This progression suggests that strong SH cyclones can emerge as secondary cyclones on the trailing cold front of pre-existing primary cyclones located to the south-east of the secondary cyclone position.

Figures 2d–2f show the 925 hPa equivalent potential temperature, depicting a north-south temperature gradient with warm air toward the equator and cooler air toward the south pole. The amplitude of the wave in the meridional temperature gradient increases as the cyclone develops. At maximum intensity the cyclonic motion associated with the cyclone has caused an overturning of the 295 K equivalent potential temperature contour suggesting the formation of a warm seclusion as cold air wraps around to the north of the cyclone center. Overlaid on the

925 hPa potential temperature and TCWV contours are the approximate positions of the composite cyclone cold and warm fronts. Figures 2g–2i illustrate the composite total column water vapor (TCWV) distribution. The highest values of TCWV are found in the warm sector of the cyclone with a filament of high TCWV ahead of the cyclone cold front, which is most pronounced 24 hr before maximum intensity. At maximum intensity, the TCWV within the cyclone warm sector starts to decrease.

4. Moisture Efficiencies

To understand the factors that influence the evolution of TCWV, we examine the water vapor budget centered on the cyclone. We measure the change in moisture content in each column of air around the cyclone center over a 6-hr period and express it as a percentage of the moisture content at the start of the 6-hr period. The moisture efficiencies are described in Section 2.5 (Equation 3).

Figures 3a–3c show that during the early stage of the cyclone's lifecycle, the PE is greater than −12%/6 hr close to the cyclone center. The PE increases as the cyclone intensifies, reaching a maximum of −60%/6 hr along the bent back warm front surrounding the cyclone center at maximum intensity (Figure 3c). This is consistent with the precipitation efficiencies calculated by Guo et al. (2015). Precipitation efficiencies of −12%/6 hr to −24%/6 hr also extend 1,000 km away from the cyclone center in a comma shaped pattern aligned with the cold front. The EE is smaller than the largest PE, but the area of moderate evaporation efficiencies (12%–24%/6 hr) is much more extensive and is located behind the cold front in the cyclone's cold sector (Figures 3d–3f).

The evolution of MFC efficiency is shown in Figures 3g–3i. During the early stage of the cyclone's evolution (48 hr before maximum intensity) columns behind the cold front experience up to 10% drying every 6 hr, while columns ahead of the cold front become up to 10% moister every 6 hr (Figure 3g). Decomposition of the MFC into terms related to advection and divergence of the flow (not shown) reveals that this dipole structure occurs because during the early stage of the cyclone's evolution the cold front moves faster than the cyclone, causing relative advection of the cold front moisture gradient. However, close to the cyclone center, positive MFC efficiency is observed throughout the cyclone's development, reaching a maximum of 55%/6 hr at maximum intensity (Figure 3i). Close to the cyclone center (within 500 km) on average 14% of the moisture converges into the cyclone every 6 hr due to MFC, offsetting the −25%/6 hr moisture lost via precipitation. The MFC decomposition (not shown) reveals that this MFC occurs because during the developing stage of cyclone evolution, the cyclone velocity is faster than the environmental wind velocity at low levels, leading to mass convergence along the cold front airmass boundary, particularly where the cold front is perpendicular to the direction of cyclone velocity (which is left to right in the rotated composite cyclones). Therefore, MFC at the tip of the filament of high TCWV in the warm sector extends the filament in the direction of cyclone propagation, which is typically toward the poles. Therefore, MFC occurring close to the cyclone center (at the head of the atmospheric river), extends the filament of high TCWV in the direction of cyclone propagation.

The sum of positive MFC efficiency and EE at the at the tip of the filament of high TCWV offsets the large negative PE resulting in decreases in TCWV of approximately −4% over 6 hr (Figures 3k and 3l). Along the remainder of the atmospheric river the MFC efficiency is negative since moisture diverges out of these columns, thus enhancing the drying caused by precipitation as the cyclone reaches maximum intensity.

5. Cyclone Airflows

In this section, we examine the vertically integrated water vapor transport (IVT) to determine the low-level cyclone airflows responsible for the flux of moisture. Where IVT is calculated using Equation 6,

$$I\vec{V}T = -\frac{1}{g} \int_{p_1}^{p_2} q\vec{u}\,dp. \tag{6}$$

IVT is vertically integrated from $p_1 = 1,000$ hPa to $p_2 = 200$ hPa. q is the specific humidity in units of kg kg^{-1}, g is the acceleration due to gravity in units of m s^{-2} and $\vec{u}$ is the horizontal wind vector in units of m s^{-1}. Figures 4a–4c illustrate the Earth-relative IVT. The warm sector of the cyclone, where moisture is highest and the cold front low-level jet is located, has the largest Earth-relative IVT. The cyan color in Figures 4a–4d corresponds to IVT >250 kg m^{-1} s^{-1}, which is typically used to identify atmospheric rivers. Therefore, even in this
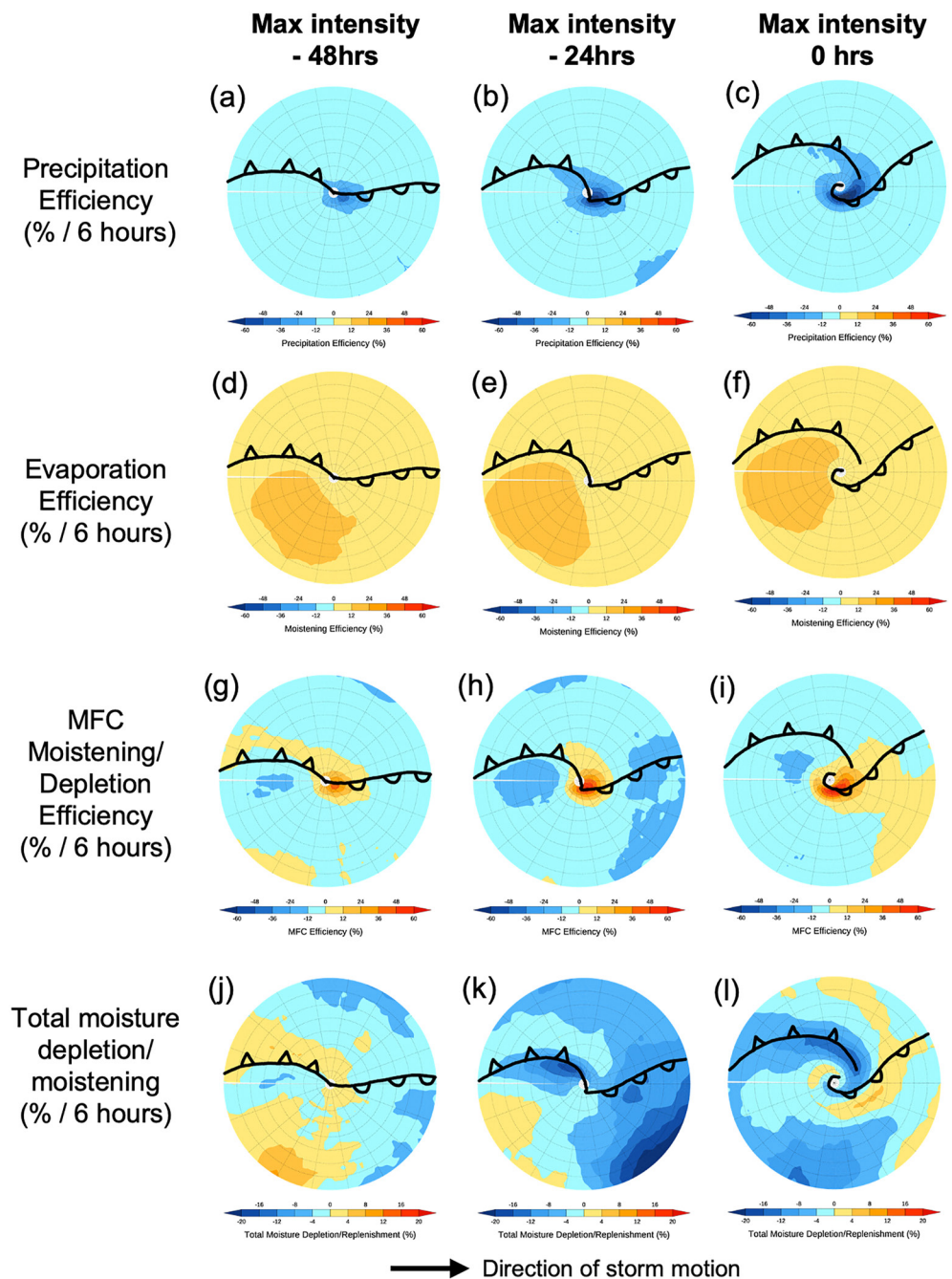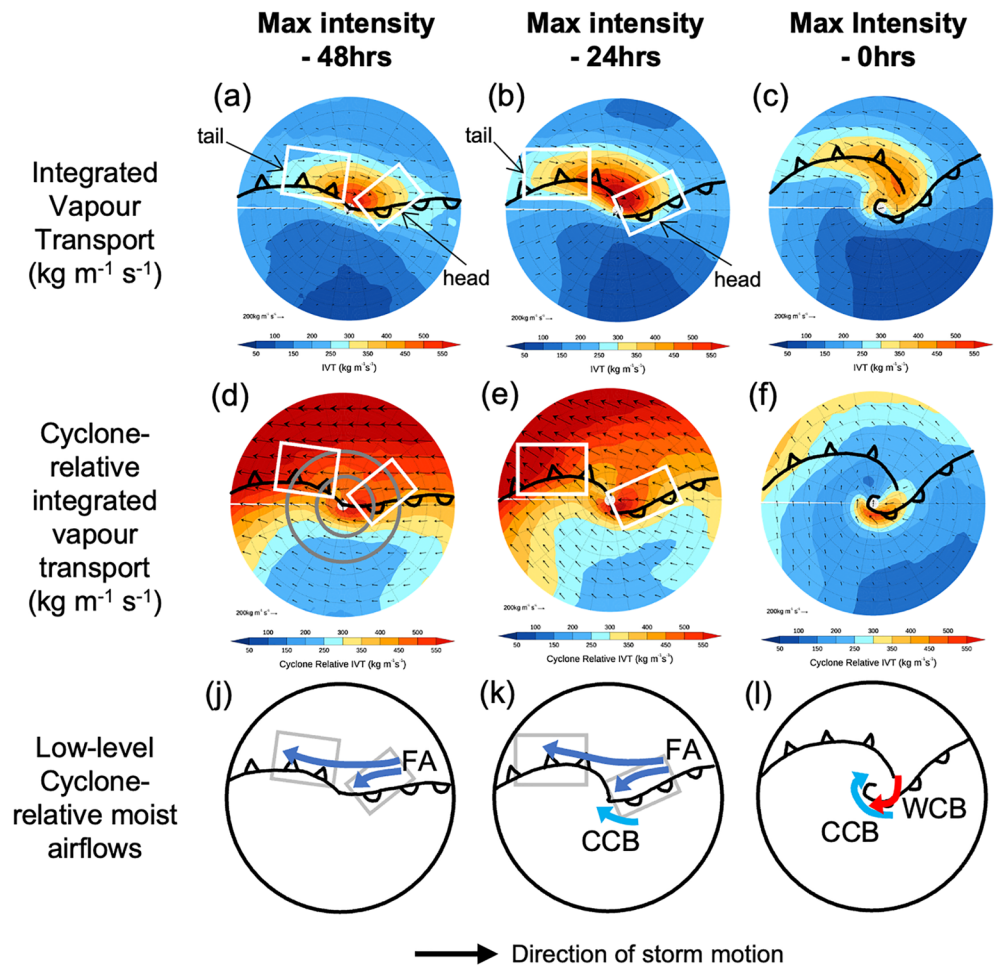
Figure 3. Evolution of cyclone centered composite terms in the moisture budget expressed as a percentage of the initial moisture content for a 6-hr period (%/6 hr). (a–c) Precipitation efficiency, (d–f) evaporation efficiency, (g)–(i) Moisture flux convergence efficiency and total moisture efficiency.

composite cyclone, an atmospheric river extends along the cold front. The IVT vectors show that moisture in the atmospheric river is transported polewards in a south-eastwards direction.

To assess the origin of moisture converging into the center of the cyclone it is necessary to compute the cyclone-relative winds by subtracting the cyclone's propagation velocity from the Earth-relative winds. The composite cyclone-relative IVT during the developing stage of the cyclone evolution is shown in Figures 4d–4f. At the head of the atmospheric river (white/gray boxes in Figure 4), the cyclone-relative vertically integrated moisture flux has a component toward the cyclone center from the direction in which the cyclone is moving.

Figure 4. Evolution of cyclone centered composite vertically integrated moisture transport (kg m^{-1} s^{-1}) using (a–c) Earth-relative winds and (d–f) cyclone relative winds. IVT flux (vectors) and IVT magnitude (filled contours). White/gray boxes indicate the head and tail of the atmospheric river. Gray circles indicate radial distances 500 and 1,000 km from the cyclone center. Panels (j–l) are schematics showing the cyclone-relative low-level moist airflows at different stages of the composite cyclone evolution. Cold conveyor belt (CCB), warm conveyor belt (WCB) and feeder airstream (FA).

Further from the cyclone center along the tail of the atmospheric river, the direction of the cyclone-relative IVT flux vectors is opposite to the Earth-relative IVT. This reversal occurs because the low-level winds are typically slower than the moving cyclone. Thus the atmospheric river consists of a head, where the moisture flux has a component toward the cyclone center and a tail where the moisture flux has a component away from the cyclone center. The FA is the low-level cyclone airflow responsible for this partition (Figures 4j and 4k).

By maximum intensity the strength of the atmospheric river has reduced since the TCWV in the warm sector reduces significantly as the cyclones travel toward the South pole (Figure 4c). The velocity of the cyclone is now similar to the atmospheric flow in which it is embedded so the cyclone-relative IVT in the warm sector is small (Figure 4f). The largest cyclone-relative IVT is found wrapping around the cyclone center, co-located with the bent-back warm front. The low-level cyclone airflow resulting in this moisture flux is known as the cold conveyor belt (CCB) (Carlson, 1980). The CCB is located on the poleward side of the cyclone center. This air is cold and dense and thus the CCB airflow has a low potential temperature and is found in the lower-troposphere (not shown). The CCB wraps cyclonically around the cyclone center and leads to the emergence of the rearward traveling (with respect to the cyclone motion) cloud head. The mid-level cyclone airflow contributing to the largest cyclone-relative IVT is known as the WCB (Browning, 1971). The WCB is a warm and moist airflow that originates on the equatorward side of the cyclone center. This airflow ascends along a sloping isentropic surface over the warm front to the mid and upper-levels of the atmosphere where it cools and releases moisture forming
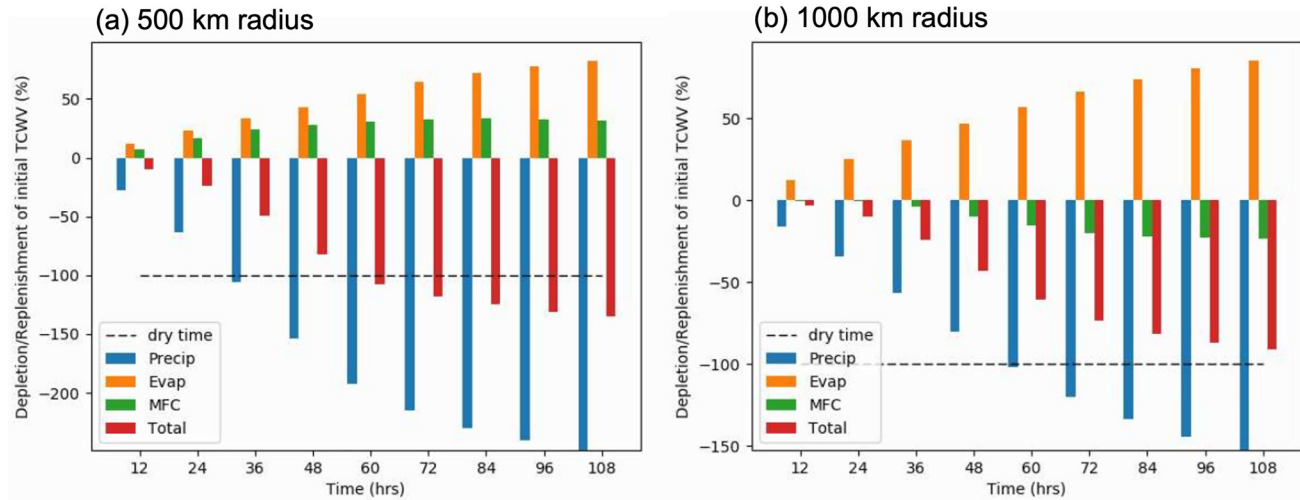
Figure 5. Composite cumulative moisture efficiency terms for 400 SH extratropical cyclones relative to the TCWV at the cyclogenesis location. The individual terms are integrated over an area surrounding the cyclone center with radius (a) 500 km and (b) 1,000 km. Cumulative precipitation efficiency (blue), evaporation efficiency (orange), moisture flux convergence efficiency (green) and total budget (red). The total budget is equal to the sum of the individual moisture efficiencies. The precipitation and general depletion timescales correspond to the times at which the blue and red bars cross the dashed line.

clouds and precipitation. One branch of the WCB turns cyclonically at mid-levels and contributes to the upper-part of the cyclones cloud head (not shown) (Figure 4l).

6. Depletion and Replenishment

In this section, we determine how long it would take for all of the column moisture at the cyclogenesis time to be lost due to precipitation. The cyclogenesis time corresponds to the first point of each individual cyclone track where the 850 hPa relative vorticity exceeds $1 \times 10^{-5} \text{s}^{-1}$. Figure 5a shows the mean cumulative PE integrated within 500 km of the cyclone center (blue bars) for increasing accumulation times. The time at which this equals -100% is equivalent to the PDT (Equation 4). Close to the cyclone center the average PDT is between 24 and 36 hr indicating that if there were no replenishment of moisture the center of the cyclone would completely dry out on a timescale of approximately 30 hr from the genesis time. The cumulative EE integrated within 500 km of the cyclone center (orange bar) is initially relatively small, but increases fairly linearly with time. Thus the integrated evaporation close to the cyclone center replenishes on average 33% of the moisture lost due to precipitation over the first 36 hr and continues to replenish the moisture throughout the cyclone evolution. The cumulative MFC efficiency close to the cyclone center (green bars) is positive close to the cyclone center and it replenishes on average 24% of moisture lost due to precipitation over the first 36 hr. The general depletion timescale, GDT, (sum of the blue, orange and green bars) is shown in the red bar. The time at which this equals -100% is equivalent to the general depletion timescale (Equation 5). The result of replenishment of moisture via evaporation and MFC as the cyclone travels extends the time taken for the cyclone center to dry out from 30 hr to between 60 and 72 hr. Thus, on average, local evaporation and MFC more than doubles the precipitating phase near the cyclone center. This ensures that there is sufficient moisture for precipitation by the time cyclones have traveled from their genesis location to their location at maximum intensity.

Figure 5b shows the average cumulative PE integrated within 1,000 km of the cyclone center. The cumulative PE (blue bars) grows at a slower rate than when integrated over 500 km since high precipitation is concentrated close to the cyclone center. As a result the PDT is longer for this larger area between 48 and 60 hr. The cumulative EE integrated within 1,000 km of the cyclone center is positive and increases throughout the cyclone lifecycle, replenishing approximately 50% of the moisture over the first 36 hr after the genesis time. Interestingly, the cumulative MFC efficiency term is negative when integrated over this 1,000 km area. This implies that there is divergence of moisture from the cyclone depleting the moisture available for precipitation. Over the first 36 hr 4% of moisture diverges from the 1,000 km surrounding the cyclone. This occurs largely because the cyclone is traveling faster than the flow in which it is embedded. This divergence of moisture is consistent with Figures 4j

and 4k which show the low-level cyclone-relative airflows during the developing stages of the cyclone evolution. The cyclonically turning branch of the feeder-airstream acts to export moisture from the cyclone center, accelerating the general depletion timescale within the tail of the atmospheric river. The system relative IVT (Figures 4d and 4e) suggest that evaporation behind the cold front is not available to the cyclone to extend its precipitating phase. Therefore, it should be noted that including the contribution from evaporation in this region will likely result in a slight overestimation of the GDT.

7. Conclusions

In this study we evaluate the composite structure of a climatology of 400 Southern Ocean extratropical cyclones and estimate their precipitation efficiencies. We find that, on average, the cyclones' maximum precipitation occurs 24 hr prior to maximum dynamical intensity. At this time there is a filament of high TCWV aligned with the composite cyclone cold front and a well-defined maximum in IVT within warm sector. The PE (ratio of 6-hourly precipitation accumulation to TCWV at the start of the 6-hr window) is largest close to the cyclone center and increases as the cyclone intensifies reaching a maximum of $-60\%/6$ hr at maximum intensity. We determine how long it would take to deplete all of a cyclone's initial moisture supply. If there were no replenishment of moisture along the cyclone's track then we find that within 500 km of the cyclone center all of the initial moisture content would be lost due to precipitation within 24–36 hr (averaged over 400 SH cyclones). However, close to the cyclone center both evaporation and MFC into the center of the cyclone replenishes the moisture lost via precipitation. This extends the precipitating phase of the cyclone from 24-36 hr to 60–72 hr after cyclogenesis. During the developing stage of cyclone evolution, moisture flux into the center of the cyclone originates ahead of the cyclone and is swept up by the cyclone as it travels through the moist environment. At the cold front some of this moisture is transported toward the center of the cyclone by the anticyclonic branch of the FA. During the mature stage of cyclone evolution the cyclone propagation speed reduces and moisture flux toward the cyclone center occurs to the south of the cyclone in the low-level CCB airstream. Further from the cyclone center ($>$500 km) moisture diverges out of the cyclone enhancing the drying caused by precipitation. In the tail of the atmospheric river moisture is transported away from the center of the cyclone by the cyclonic branch of the FA and is left behind to form the atmospheric river footprint.

Data Availability Statement

The composite fields associated with over 400 Southern Ocean extratropical cyclones are freely available via the Extratropical Cyclone Atlas (H. Dacre et al., 2011).

References

Bengtsson, L., Hodges, K. I., & Keenlyside, N. (2009). Will extratropical storms intensify in a warmer climate? *Journal of Climate*, *22*(9), 2276–2301. https://doi.org/10.1175/2008jcli2678.1

Booth, J. F., Naud, C. M., & Jeyaratnam, J. (2018). Extratropical cyclone precipitation life cycles: A satellite-based analysis. *Geophysical Research Letters*, *45*(16), 8647–8654. https://doi.org/10.1029/2018gl078977

Browning, K. (1971). Radar measurements of air motion near fronts. *Weather*, *26*(8), 320–340. https://doi.org/10.1002/j.1477-8696.1971.tb07416.x

Browning, K., & Harrold, T. (1970). Air motion and precipitation growth at a cold front. *Quarterly Journal of the Royal Meteorological Society*, *96*(409), 369–389. https://doi.org/10.1002/qj.49709640903

Bui, H., & Spengler, T. (2021). On the influence of sea surface temperature distributions on the development of extratropical cyclones. *Journal of the Atmospheric Sciences*, *78*(4), 1173–1188. https://doi.org/10.1175/jas-d-20-0137.1

Carlson, T. N. (1980). Airflow through midlatitude cyclones and the comma cloud pattern. *Monthly Weather Review*, *108*(10), 1498–1509. https://doi.org/10.1175/1520-0493(1980)108<1498:atmcat>2.0.co;2

Catto, J. L., Shaffrey, L. C., & Hodges, K. I. (2010). Can climate models capture the structure of extratropical cyclones? *Journal of Climate*, *23*(7), 1621–1635. https://doi.org/10.1175/2009jcli3318.1

Cuckow, S., Dacre, H. F., & Martínez-Alvarado, O. (2022). Moisture transport contributing to precipitation at the centre of storm Bronagh. *Weather*, *77*(6), 196–201. https://doi.org/10.1002/wea.4212

Dacre, H., Hawcroft, M., Stringer, M., & Hodges, K. (2011). Extratropical cyclone atlas [Dataset]. https://www.met.rdg.ac.uk/~storms

Dacre, H., Hawcroft, M., Stringer, M., & Hodges, K. (2012). An extratropical cyclone atlas: A tool for illustrating cyclone structure and evolution characteristics. *Bulletin of the American Meteorological Society*, *93*(10), 1497–1502. https://doi.org/10.1175/bams-d-11-00164.1

Dacre, H. F., Clark, P. A., Martinez-Alvarado, O., Stringer, M. A., & Lavers, D. A. (2015). How do atmospheric rivers form? *Bulletin of the American Meteorological Society*, *96*(8), 1243–1255. https://doi.org/10.1175/bams-d-14-00031.1

Dacre, H. F., Martínez-Alvarado, O., & Mbengue, C. O. (2019). Linking atmospheric rivers and warm conveyor belt airflows. *Journal of Hydrometeorology*, *20*(6), 1183–1196. https://doi.org/10.1175/jhm-d-18-0175.1

Dacre, H. F., & Pinto, J. G. (2020). Serial clustering of extratropical cyclones: A review of where, when and why it occurs. *npj Climate and Atmospheric Science*, *3*(1), 48. https://doi.org/10.1038/s41612-020-00152-9

Demirdjian, R., Doyle, J. D., Finocchio, P. M., & Reynolds, C. A. (2022). On the influence of surface latent heat fluxes on idealized extratropical cyclones. *Journal of the Atmospheric Sciences*, *79*(9), 2229–2242. https://doi.org/10.1175/jas-d-22-0035.1

Eiras-Barca, J., Dominguez, F., Hu, H., Garaboa-Paz, D., & Miguez-Macho, G. (2017). Evaluation of the moisture sources in two extreme landfalling atmospheric river events using an Eulerian WRF tracers tool. *Earth System Dynamics*, *8*(4), 1247–1261. https://doi.org/10.5194/esd-8-1247-2017

Ferrier, B. S., Simpson, J., & Tao, W.-K. (1996). Factors responsible for precipitation efficiencies in midlatitude and tropical squall simulations. *Monthly Weather Review*, *124*(10), 2100–2125. https://doi.org/10.1175/1520-0493(1996)124<2100:frfpei>2.0.co;2

Guo, C., Xiao, H., Yang, H., & Tang, Q. (2015). Observation and modeling analyses of the macro-and microphysical characteristics of a heavy rain storm in Beijing. *Atmospheric Research*, *156*, 125–141. https://doi.org/10.1016/j.atmosres.2015.01.007

Hersbach, H., Bell, B., Berrisford, P., Hirahara, S., Horányi, A., Muñoz-Sabater, J., et al. (2020). The ERA5 global reanalysis. *Quarterly Journal of the Royal Meteorological Society*, *146*(730), 1999–2049. https://doi.org/10.1002/qj.3803

Hobbs, P. V., Matejka, T. J., Herzegh, P. H., Locatelli, J. D., & Houze, R. A. (1980). The mesoscale and microscale structure and organization of clouds and precipitation in midlatitude cyclones. I: A case study of a cold front. *Journal of the Atmospheric Sciences*, *37*(3), 568–596. https://doi.org/10.1175/1520-0469(1980)037<0568:tmamsa>2.0.co;2

Hodges, K. (1995). Feature tracking on the unit sphere. *Monthly Weather Review*, *123*(12), 3458–3465. https://doi.org/10.1175/1520-0493(1995)123<3458:ftotus>2.0.co;2

Hoskins, B. J., & Hodges, K. I. (2005). A new perspective on Southern Hemisphere storm tracks. *Journal of Climate*, *18*(20), 4108–4129. https://doi.org/10.1175/jcli3570.1

Hu, H., & Dominguez, F. (2019). Understanding the role of tropical moisture in atmospheric rivers. *Journal of Geophysical Research: Atmospheres*, *124*(24), 13826–13842. https://doi.org/10.1029/2019jd030867

Lavers, D. A., Simmons, A., Vamborg, F., & Rodwell, M. J. (2022). An evaluation of ERA5 precipitation for climate monitoring. *Quarterly Journal of the Royal Meteorological Society*, *148*(748), 3152–3165. https://doi.org/10.1002/qj.4351

Li, X., Sui, C.-H., & Lau, K.-M. (2002). Precipitation efficiency in the tropical deep convective regime: A 2-D cloud resolving modeling study. *Journal of the Meteorological Society of Japan. Ser. II*, *80*(2), 205–212. https://doi.org/10.2151/jmsj.80.205

Lutz, J. T. (1977). Precipitation efficiency under varying atmospheric conditions. *Geographical Bulletin*, *14*, 16.

Newell, R. E., Newell, N. E., Zhu, Y., & Scott, C. (1992). Tropospheric rivers? A pilot study. *Geophysical Research Letters*, *19*(24), 2401–2404. https://doi.org/10.1029/92gl02916

Papritz, L., Aemisegger, F., & Wernli, H. (2021). Sources and transport pathways of precipitating waters in cold-season deep North Atlantic cyclones. *Journal of the Atmospheric Sciences*, *78*(10), 3349–3368. https://doi.org/10.1175/jas-d-21-0105.1

Pfahl, S., & Sprenger, M. (2016). On the relationship between extratropical cyclone precipitation and intensity. *Geophysical Research Letters*, *43*(4), 1752–1758. https://doi.org/10.1002/2016gl068018

Rea, D., Rauber, R. M., Hu, H., Tessendorf, S. A., Nesbitt, S. W., Jewett, B. F., & Zaremba, T. J. (2023). The contribution of subtropical moisture within an atmospheric river on moisture flux, cloud structure, and precipitation over the Salmon River Mountains of Idaho using moisture tracers. *Journal of Geophysical Research: Atmospheres*, *128*(6), e2022JD037727. https://doi.org/10.1029/2022jd037727

Sinclair, V., & Dacre, H. (2019). Which extratropical cyclones contribute most to the transport of moisture in the Southern Hemisphere? *Journal of Geophysical Research: Atmospheres*, *124*(5), 2525–2545. https://doi.org/10.1029/2018jd028766

Sodemann, H., & Stohl, A. (2013). Moisture origin and meridional transport in atmospheric rivers and their association with multiple cyclones. *Monthly Weather Review*, *141*(8), 2850–2868. https://doi.org/10.1175/mwr-d-12-00256.1

Stewart, R. E. (1996). Extratropical cyclones: Their mesoscale structure, precipitation and role in the transport of water. In *Radiation and water in the climate system: Remote measurements* (pp. 129–148). Springer.

Tuller, S. E. (1971). The world distribution of annual precipitation efficiency. *Journal of Geography*, *70*(4), 219–223. https://doi.org/10.1080/00221347108981623

Xu, G., Wang, L., Chang, P., Ma, X., & Wang, S. (2022). Improving the understanding of atmospheric river water vapor transport using a three-dimensional straightened composite analysis. *Journal of Geophysical Research: Atmospheres*, *127*(11), e2021JD036159. https://doi.org/10.1029/2021jd036159